INTERNATIONAL JOURNAL FOR NUMERICAL METHODS IN FLUIDS, VOL. 8, 943–955 (1988)

AXIALLY SYMMETRIC CAVITATION FLOW AT SMALL CAVITATION NUMBERS

A. DAGAN

MOD Scientific Department, Division 46, P.O. Box 2250, Haifa, 31021, Israel

SUMMARY

A method for computing the drag coefficient of a body in an axially symmetric, steady-state cavitation flow is presented. A 'vortex ring' distribution along the wetted body surface and along the cavity interface is assumed. Since the location of the cavitation interface is unknown *a priori*, an iterative procedure is used, where, for the first stage, an arbitrary cavitation interface is assumed. The flow field is then solved, and by an iterative process the location of the cavitation interface is corrected. Even though the flow field is governed by the linear Laplace equation, strong non-linearity resulting from the kinematic boundary conditions appears along the cavitation interface. An improved numerical scheme for solving the dual Fredholm integral equations is obtained by formulating high-order approximations to the singular integrals in order to reduce the matrix dimensions. Good agreement is found between the numerical results of the present work, experimental results and other solutions.

KEY WORDS Cavitation flow Cavitation number Singular integrals Boundary integral method

INTRODUCTION

Cavitation flow appears in many hydrodynamic problems and its impact on engineering design is of primary interest. In particular, much concern has been devoted over the last 20 years to two-dimensional cavitating hydrofoils. Many similarities exist between the two-dimensional problem and the axially symmetric one. The potential flow assumption is the common ground between the various methods for solving such flows. However, no direct method for solving the axially symmetric case has been suggested. This is because of the non-linearity resulting from the kinematic boundary condition along the cavity interface and the unknown location of the cavity interface itself. An exception is the work of Garabedian[1] who solves the axisymmetric case by applying an asymptotic correction to the two-dimensional flow.

Because of the numerical difficulties encountered while solving the axially symmetric cavitation flow in the physical domain, Brennen[2] has transformed the physical system to (ϕ, ψ)-co-ordinates (potential and stream function respectively). This transformation removes the geometrical complexity in the physical domain due to the fact that both the wetted part of the body and the cavity interface appear as a single streamline in the transformed plane. However, the transformed form of the Laplace equation is non-linear, therefore an iterative point technique is used in order to solve the equation numerically.

In the same way Mogel and Street[3] propose a traditional iterative method for computing the two-dimensional cavitation flow behind the plate. The first stage of this method assumes an arbitrary initial location for the cavity interface. Laplace's equation is solved in the physical plane

0271–2091/88/080943–13$06.50

Received 27 July 1987
Revised 20 November 1987

using a second-order, finite difference approximation, while applying the boundary conditions of constant pressure on the cavity interface and zero normal velocity on the plate. The assumed cavity interface is then corrected by using the kinematic boundary condition (zero mass flux across the interface).

One of the most effective methods for calculating the flow over fully immersed bodies uses distributions of potential singularities along the body surface. This method is known as the 'boundary integral method'. This class of singularities includes vortex (or dipole) and source distributions. The main computational complication involved in such methods is the appearance of singular integrals. The work of Armstrong and Dunham[4] can be classified in this category. Here the cavity interface as well as the wetted body is replaced by a 'vortex ring' distribution, and the interface location is corrected by an iterative process. Since the application of this method requires large and fast computers, the authors present only a simplified, approximate solution.

Since a finite difference approximation to these singular integrals leads to full matrices, a high-order truncation error is required to reduce the matrix dimensions. Moreover, owing to the singularity in the integrand, the traditional numerical methods are not capable of evaluating such integrals properly. One way to remove this difficulty is to represent the regular terms within the integrand by the use of the spline-fit method.[5] This method enables one to solve an arbitrary body within the flow field to a high degree of approximation or, alternatively, with predetermined precision, to reduce the matrix dimensions. However, the authors of Reference 5 preferred to use a numerical integration in each interval rather than reduce the computation time by computing these integrals analytically.

There are some approximate solutions related to cavity flows where the wetted body together with the cavity interface are represented by an ellipsoid.[6]

MATHEMATICAL MODEL AND BOUNDARY CONDITIONS

The potential flow assumption is commonly used to describe the flow field in cavitation flow. i.e.

$$\nabla^2\phi = 0.$$

This flow field description fits the front part of the cavity interface well, but fails to describe the rear part, which is turbulent.[2] The appearance of turbulence in the rear part of the cavity interface is due to the cavity closure. Therefore the potential flow assumption is physically unrealistic in this region, where in addition such an assumption leads to a contradiction. On one hand the pressure along the cavity interface is supposed to be the vapour pressure, and on the other hand cavity closure will require a stagnation point at the closure point, i.e. stagnation pressure. Thus a possible mechanism behind the closure of the cavity interface is the appearance of a fully wetted wake in which the pressure is gradually recovered from the vapour pressure to the free stream pressure. In practice, the closure region is marked by considerable turbulence and some local unsteadiness.[2] In order to remove the 'closure point problem' several models exist, of which the simplest and most widely used is the Riabouchinski model[7] in which longitudinal symmetry about the plane of maximum diameter of the cavity is assumed.

An important point is the nature of the separation point (the point where the cavity interface separates from the wetted body). The separation is abrupt whenever the wetted body contains a slope discontinuity and is considered to be smooth otherwise. However, the cavity separation is essentially a viscous phenomenon[8] and takes place when the wetted-body shear stress becomes zero.[2,9] The classical condition for smooth separation requires that the curvature of the free streamline be finite at the separation, in which case it can be shown to be equal to the curvature of the solid body at the detachment point.[4] This condition does not take into account real-fluid

effects on the position of the cavitation separation due to viscosity. Brennen[2] has shown that the position of the cavitation separation on smooth bodies depends at least on the Reynolds number. Flow visualization in the neighbourhood of the fully developed cavity on axisymmetric head forms has shown the existence of laminar boundary layer separation upstream of cavitation separation, and the distance between the two depends strongly on the Reynolds number. On the basis of this result Arakeri[8] developed a semi-empirical method to predict the position of cavitation separation on smooth bodies. In the present study an abrupt separation, or a smooth separation, where the separation location is known *a priori*, is considered. As is pointed out in Reference 4, the singularity in the separation point curvature should be taken into account, otherwise no solution can be expected. Therefore the correct representation of the cavity interface is a vortex sheet distributed along the cavity interface and along the wetted nose, where the singularity in the separation point curvature will appear in the vortex sheet strength at the separation point.

By using Green's theorem, the velocity potential of an arbitrary point within the flow field can be written as

$$\phi(x_1, y_1, z_1) = -\iint_B \frac{\partial \phi}{\partial n} \frac{1}{4\pi R} \mathrm{d}A + \iint_B \phi \frac{\partial}{\partial n}\left(\frac{1}{4\pi R}\right) \mathrm{d}A. \tag{1}$$

The integration region denoted by B is taken over the wetted body and over the cavity interface, ϕ is the potential function, R is the radial distance from B to an arbitrary point (x_1, y_1, z_1), $\partial/\partial n$ is the derivative normal to the boundary element $\mathrm{d}A$ and ϕ_0 is the far-field potential. The first integral represents a source–sink distribution, while the second one describes a distribution of doublets with axes normal to B. By assuming that $\partial\phi/\partial n$ is continuous across the interface and across the wetted nose (Neumann condition),[10] equation (1) reduces to the following form:

$$\phi - \phi_0 = \iint_B \phi^* \frac{\partial}{\partial n}\left(\frac{1}{4\pi R}\right) \mathrm{d}A. \tag{2}$$

In such a case an artificial flow field is generated within the closed region described by the cavity interface and the wetted nose, where ϕ is now discontinuous across the boundary. Hence $\phi^* = \phi_{\text{out}} - \phi_{\text{in}}$, where ϕ_{out} is the outer potential along the boundary and ϕ_{in} is the inner potential along the boundary. On B the last equation reduces to the following form:

$$\tfrac{1}{2}\phi_B - \phi_0 = \iint_B \phi^* \frac{\partial}{\partial n}\left(\frac{1}{4\pi R}\right) \mathrm{d}A. \tag{3}$$

By dividing the body surface into small elements of constant dipole strength and taking into account the fact that a dipole with constant strength can be replaced by a vortex ring around the boundary of the dipole element, the following expression is obtained:

$$u_B = \tfrac{1}{2} V_s(\mathbf{1}_x \cos\theta + \mathbf{1}_R \sin\theta) - \frac{1}{4\pi}\int_0^{s_1} v_s(e_x \mathbf{1}_x + e_R \mathbf{1}_R)\,\mathrm{d}S,$$

where

$$e_x = \frac{1}{\sqrt{[(x-x_1)^2 + (R+r)^2]}}\left[\left(\frac{R+r}{r}k^2 - 2\right)\frac{E(k^2)}{1-k^2} + 2K(k^2)\right],$$

$$e_R = \frac{1}{\sqrt{[(x-x_1)^2 + (R+r)^2]}}\frac{1}{r}\left(\frac{2-k^2}{1-k^2}E(k^2) - 2K(k^2)\right), \tag{4}$$

$$k^2 = \frac{4Rr}{(x-x_1)^2 + (R+r)^2}.$$

Here E is the complete elliptic integral of the second kind, K is the complete elliptic integral of the first kind and θ is the inclination angle of the tangent to the meridian section of the surface relative to the longitudinal axis.[5] We define the boundary co-ordinates (s, ξ) as follows (Figure 1):

$$\begin{aligned} R(s) &= \int_0^s \sin\theta(v)\,\mathrm{d}v, \qquad r(\xi) = \int_0^\xi \sin\theta(v)\,\mathrm{d}v, \\ x_1(s) &= \int_0^s \cos\theta(v)\,\mathrm{d}v, \qquad x(\xi) = \int_0^\xi \cos\theta(v)\,\mathrm{d}v. \end{aligned} \tag{5}$$

These co-ordinates are preferable for solving equation (4). By using equations (4) and (5), the asymptotic behaviour of the leading terms of the induced coefficients (e_x, e_R) in the vicinity of the singular point $(s\to\xi,\ x\to x_1,\ R\to r,\ k^2\to 1)$ is

$$\begin{aligned} e_x(s\to\xi) &= 2\sin\theta/(s-\xi) + 2K(k^2\to 1)/2r, \\ e_R(s\to\xi) &= -2\cos\theta/(s-\xi). \end{aligned} \tag{6}$$

Hence the leading terms of the asymptotic expansion behave like $1/(s-\xi)$ in the vicinity of the singularity, or, in another words, the leading terms behave similarly to the two-dimensional solution resulting from a Cauchy integral in the complex plane. This singularity should be taken into consideration when an appropriate numerical scheme for such integrals is developed. This point will be discussed in the next section.

The integral equation (4) is essentially the Dirichlet-type solution of (1) for a given tangential velocity on B. In a steady-state cavitation flow the boundary B is considered as a single stream surface. Therefore the kinematic boundary condition along B can be expressed as follows:

$$\frac{\mathrm{d}}{\mathrm{d}t}[R - R(x_1)] = \bar{v}\nabla[R - R(x_1)] = v_r - \frac{\mathrm{d}R}{\mathrm{d}x}v_x = 0,$$

where v_r and v_x are the velocity components in the radial and horizontal directions respectively. By applying Bernoulli's law and assuming constant pressure along the cavity interface, the dynamic boundary condition can be easily evaluated as

$$\frac{P_\infty - P_v}{\frac{1}{2}\rho_w V_\infty^2} = v_s^2 - 1,$$

where P_v is the vapour pressure, P_∞ is the hydrostatic pressure and ρ_w is the liquid density. The term $(P_\infty - P_v)/\frac{1}{2}\rho_w V_\infty^2$ is also defined as the cavitation number σ. For cavitation flows for which $\sigma \neq 0$, several models can be used,[7] but the simplest and most widely used is the model of Riabouchinski mentioned previously. The asymptotic cavity length for a small cavitation number

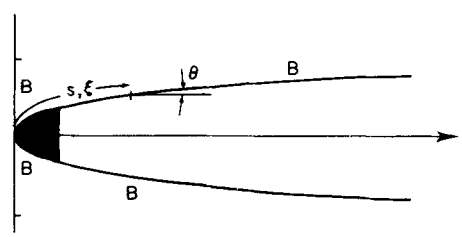

Figure 1. Schematic description of the boundary B and the co-ordinates (s, ξ)

is given by

$$\left(\frac{L}{D}\right)^2 \frac{1}{C_d} \approx \frac{1}{\sigma^2} \ln \frac{1}{\sigma},$$

where L is the distance of the maximum-diameter station of the cavity from the nose and D is the diameter at the separation point. The drag coefficient C_d for a small cavitation number behaves as $C_d = C_d^{(0)} + C_d^{(1)}\sigma + \ldots$; hence for a small cavitation number the ratio $L/D \to \infty$. Consequently, an infinite cavity length is assumed in this study as a model for a small-cavitation-number flow.

The kinematic boundary condition on B can be rearranged as follows:

$$(1+u)\sin\theta - v_r \cos\theta = 0.$$

Upon substitution, the following equation is obtained:

$$\frac{1}{4\pi}\int_0^{s_1} v_s(s)[e_x(s,\xi)\sin\theta(\xi) - e_R(s,\xi)\cos\theta(\xi)]\,ds = \sin\theta(\xi), \tag{7}$$

where s_1 is the arc length of B.

The tangential velocity must be equal to the vortex density along B, yielding

$$(1+u)\cos\theta + v_r \sin\theta = v_s$$

or

$$\frac{1}{2}v_s + \frac{1}{4\pi}\int_0^{s_1} v_s(s)[e_x(s,\xi)\cos\theta(\xi) + e_R(s,\xi)\sin\theta(\xi)]\,ds = \cos\theta(\xi). \tag{8}$$

Equation (7) is a Fredholm integral of the first kind while equation (8) is of the second kind.[5]

NUMERICAL SCHEMES

Ordinary integration schemes fail to properly evaluate the singular integrals (presented in the previous section). Thus in this section, for clarity, we will develop and check our numerical scheme initially for a fully wetted body without a cavity. In the next section the method is extended to a flow with a cavity. In order to remove the difficulty experienced as a result of the singular integrals, the Fredholm integral equation (7) is rewritten in a different form which isolates the leading singularity:

$$\int_0^{s_1} v_s(s)[e_x(s,\xi)\sin\theta(\xi) - e_R(s,\xi)\cos\theta(\xi)]\,ds = \int_0^{s_1} \frac{q(s,\xi)}{s-\xi}\,ds, \tag{9}$$

where $q(s,\xi)$ is finite for all values of s and ξ.

The body surface is divided into $N-1$ equal intervals of length h; the function $q(s,\xi)$ is defined at each end point and is linear with respect to v_s. $q(s,\xi)$ has two stagnation points at $s=0$ and $s=(N-1)h$. In order to satisfy the boundary condition on equation (7) or (8), $N-2$ check points (ξ_j) were selected. At each check point we require the boundary condition to be fulfilled. It is clear that for an acceptable, stable numerical scheme, the results (apart from the truncation error) should not depend on the particular set of points ξ_j chosen.

In order to increase the accuracy of the proposed system, or alternatively to reduce the matrix size for a given accuracy, a high-order approximation to the integral is needed. In any such approximation, the singular behaviour of the elliptic function has to be taken into account. The

elliptic function can be expressed, with an absolute error of 10^{-5}, as follows:[11]

$$K(k^2)=K_1(k^2)\ln(1-k^2)+K_2(k^2),$$
$$E(k^2)=E_1(k^2)\ln(1-k^2)+E_2(k^2), \tag{10}$$

where

$$K_1(k^2)=-\sum_{i=0}^{2} b_i(1-k^2)^i, \qquad E_1(k^2)=\sum_{i=0}^{2} b_i^*(1-k^2)^i,$$
$$K_2(k^2)=-\sum_{i=0}^{2} a_i(1-k^2)^i, \qquad E_2(k^2)=\sum_{i=0}^{2} a_i^*(1-k^2)^i \tag{11}$$

and a_i, a_i^*, b_i, b_i^* are defined as follows:[11]

$$a_0=1{\cdot}3862944, \quad a_1=0{\cdot}1119723, \quad a_2=0{\cdot}0725296,$$
$$b_0=0{\cdot}5000000, \quad b_1=0{\cdot}1213478, \quad b_2=0{\cdot}0288729,$$
$$a_0^*=1{\cdot}0000000, \quad a_1^*=0{\cdot}4630151, \quad a_2^*=0{\cdot}1077812,$$
$$b_0^*=0{\cdot}0000000, \quad b_1^*=0{\cdot}2452727, \quad b_2^*=0{\cdot}0412496.$$

The last expressions are transformed to the boundary co-ordinates (s, ξ) in the following manner:

$$K(k^2)=\left(K_1(k^2)\ln\frac{1-k^2}{(s-\xi)^2}h^2+K_2(k^2)\right)+2K_1(k^2)\ln\frac{s-\xi}{h}=K_1^*+K_2^*\ln\frac{s-\xi}{h},$$
$$E(k^2)=\left(E_1(k^2)\ln\frac{1-k^2}{(s-\xi)^2}h^2+E_2(k^2)\right)+2E_1(k^2)\ln\frac{s-\xi}{h}=E_1^*+E_2^*\ln\frac{s-\xi}{h}.$$

In this representation K_1^*, K_2^*, E_1^* and E_2^* are regular functions. The Fredholm integral equation of the first kind can now be rewritten as

$$\frac{1}{4\pi}\int_0^{s_1}\left(\frac{f(s,\xi)}{s-\xi}+g(s,\xi)\ln\frac{s-\xi}{h}\right)\mathrm{d}s=\sin\theta, \tag{12}$$

where

$$f(s,\xi)=\frac{(s-\xi)^2}{1-k^2}\frac{1}{\sqrt{(x-x_1)^2+(R+r)^2}}\left(-\frac{x-x_1}{s-\xi}\frac{A_1(k^2)}{r}\cos\theta+\frac{B_1(k^2)}{s-\xi}\sin\theta\right)v_s(s),$$
$$g(s,\xi)=\frac{(s-\xi)^2}{1-k^2}\frac{1}{\sqrt{(x-x_1)^2+(R+r)^2}}\left(-\frac{x-x_1}{s-\xi}\frac{A_2(k^2)}{s-\xi}\frac{\cos\theta}{r}+\frac{B_2(k^2)}{(s-\xi)^2}\sin\theta\right)v_s(s),$$

and

$$A_1(k^2)=(2-k^2)E_1^*-2(1-k^2)K_1^*,$$
$$A_2(k^2)=(2-k^2)E_2^*-2(1-k^2)K_2^*,$$
$$B_1(k^2)=-A_1(k^2)+\frac{R}{r}k^2E_1^*,$$
$$B_2(k^2)=-A_2(k^2)+\frac{R}{r}k^2E_2^*.$$

Note that $f(s, \xi)$ and $g(s, \xi)$ are regular functions. The formulation of equation (12) in a finite

difference form is written as

$$\int_0^{s_1}\left(\frac{f(s,\xi)}{s-\xi}+g(s,\xi)\ln\frac{s-\xi}{h}\right)ds=\int_{-1}^{1}\left(\frac{\chi^p f_{1,j}}{\beta_{1,j}+p}+\chi^p g_{1,j}\ln(\beta_{1,j}+p)\right)dp$$
$$+\sum_{2}^{N-1}\int_0^1\left(\frac{\chi^p f_{i,j}}{\beta_{i,j}+p}+\chi^p g_{i,j}\ln(\beta_{i,j}+p)\right)dp,$$

where χ^p is represented by a central finite difference operator with truncation error of order h^3:

$$\chi^p=\exp\left(ph\frac{\partial}{\partial x}\right)=1+\frac{p}{2}\mu\delta+\frac{p^2}{2}\delta^2,$$

where

$$\mu f_i=f_{i+1/2}+f_{i-1/2}, \qquad \delta f_i=f_{i+1/2}-f_{i-1/2}$$

and where p and β are defined by

$$p=\frac{s-s_i}{h}, \qquad \beta=\frac{s_i-\xi_j}{h}.$$

The finite difference operators χ, μ, δ operate on $f_{i,j}$ and $g_{i,j}$. The above formulation reduces the Fredholm integral equation of the first kind to the following form:

$$\frac{1}{4\pi}\sum_{i=1}^{N}A_{i,j}v_i=\sin\theta_j, \quad 1<j<N. \tag{13}$$

In order to check the accuracy of this linear system, the results are compared with the exact solution for a moving sphere, with the right-hand side of equation (13) taken as the exact value. The linear system converges rapidly to the exact solution as indicated by the error (see Table I), which is proportional to the expected truncation error, of order h^3. However, near the stagnation points the error increases continuously, reaching order h^2. Numerical experiments show that selecting different sets of evenly spaced check points ξ_j produces no errors of order greater than the truncation error.

ITERATIVE PROCESS FOR THE CAVITY INTERFACE

The wetted nose and the cavity interface denoted by B are divided into small intervals as in the previous section. For the first step a cavity interface location is chosen, which is arbitrary except that a continuous slope is maintained at the separation point. Under this assumption, the Fredholm integral equation of the first kind can be written as

$$\frac{1}{4\pi}\sum_{i=1}^{N}A_{i,j}^{\kappa-1}v_i^{\kappa}+\frac{1}{4\pi}v_N^{\kappa}\sum_{i=N}^{\infty}A_{i,j}^{\kappa-1}=\frac{R_{j+1}-R_j}{h}, \quad 1<j<N. \tag{14}$$

Equation (14) is satisfied on the wetted nose, at N mesh points. The matrix $A_{i,j}$ is the same matrix as in equation (13) and is a function of the geometry of B. In order to satisfy the dynamic boundary condition, a constant velocity v_M is assumed, where v_M is the tangential velocity at the separation. Note that $V_N=v_M$ is assumed on the cavity interface. Clearly, equation (14) ensures that the wetted part of B is a stream surface. However, in order to ensure that the cavity interface

Table I. Comparison between the exact and the numerical solution for a sphere

20 points along the wetted body			
θ(rad)	Numerical	Exact	|Error|
0·6614	0·9248	0·9213	0·003490
1·3228	1·4557	1·4541	0·001579
1·9342	1·3725	1·3737	0·001193
2·6456	0·7051	0·7139	0·008831
40 points along the wetted body			
θ(rad)	Numerical	Exact	|Error|
0·3222	0·4759	0·4750	0·000860
0·6444	0·9016	0·9011	0·000444
0·9666	1·2348	1·2345	0·000323
1·2889	1·4410	1·4408	0·000211
1·6111	1·4989	1·4988	0·000077
1·9333	1·4024	1·4025	0·000084
2·2555	1·1616	1·1619	0·000292
2·5777	1·8010	0·8017	0·000691
2·8999	0·3558	0·3590	0·003156
80 points along the wetted body			
θ(rad)	Numerical	Exact	|Error|
0·1591	0·2379	0·2376	0·000323
0·3181	0·4693	0·4692	0·000108
0·4772	0·6890	0·6889	0·000066
0·6363	0·8914	0·8913	0·000052
0·7953	1·0712	1·0712	0·000048
0·9544	1·2240	1·2240	0·000047
1·1135	1·3459	1·3459	0·000048
1·2725	1·4338	1·4338	0·000051
1·4316	1·4855	1·4855	0·000054
1·5907	1.4998	0·4997	0·000059
1·7497	1·4761	1·4760	0·000066
1·9088	1·4152	1·4151	0·000076
2·0679	1·3186	1·3185	0·000091
2·2270	1·1886	1·1885	0·000115
2·3860	1·0287	1·0286	0·000157
2·5451	0·8429	0·8426	0·000236
2·7042	0·6358	0·6354	0·000417
2·8632	0·4132	0·4122	0·000985
3·0223	0·1836	0·1785	0·005111

is a stream surface too, the assumed cavity interface shape has to be corrected as follows:

$$\sin\theta^{\kappa} = \frac{v_r^{\kappa-1/2}}{v_N} = \frac{1}{2}\sin\theta^{\kappa} - \frac{1}{4\pi}\int_0^{\infty} \frac{v_s^{\kappa}}{v_N^{\kappa}} e_R^{\kappa-1}\,\mathrm{d}s,$$

where κ is the iteration counter. In a finite difference form the above equation can be written

$$\sin\theta^{\kappa}=\frac{1}{2\pi}\sum_{i=1}^{N}A_{i,j}^{\kappa-1}|_{\theta_j=0}\left(\frac{v_i}{v_N}\right)^{\kappa}+\frac{1}{2\pi}\sum_{i=N+1}^{\infty}A_{i,j}^{\kappa-1}|_{\theta_j=0}. \tag{15}$$

Clearly, it is easy to verify that only when $\theta_j=0$, $A_{i,j}$ reduces to $-e_{R,i,j}$ and the new location of the cavity interface can be obtained as follows:

$$x^{\kappa}=\int_0^s\cos\theta^{\kappa}\,ds, \qquad R^{\kappa}=\int_0^s\sin\theta^{\kappa}\,ds.$$

The above equation is computed to the same accuracy as the Fredholm integral equation, i.e. to order h^3, and the iterative procedure is repeated until convergence is obtained. In such a case B is a stream surface and the cavity interface of B also satisfies the dynamic boundary condition. The present method converges to the same solution for any form of initial cavity location, but from our experience it is preferable to take as an initial guess a parabolic interface, which is a good approximation.[9]

Only a part of the cavity interface is computed by equation (15) (about five to ten arc lengths of the wetted nose downstream of the separation). The rest of the cavity interface can be represented asymptotically according to Garabedian[1] as

$$R=\text{constant}\times S^{1/2}(\ln S)^{-1/4}.$$

The constant was found by matching the computed cavity interface to the above expression to maintain continuity.

Drag coefficient

The drag coefficient is determined directly by integration of the pressure distribution around the wetted nose, i.e.

$$C_d=\frac{F_d}{\frac{1}{2}\rho_w V_\infty^2}=\frac{2(1+\sigma)}{R_L^2}\int_0^L\left[1-\left(\frac{v_s}{v_M}\right)^2\right]R(s)\,ds, \tag{16}$$

where A_L and R_L are the cross-sectional area and radius at the separation point respectively and F_d is the drag force. The drag coefficient C_d is non-dimensionalized to the dynamic pressure of the free flow. The computation is carried out for the number of different lengths downstream of separation and in each case the resulting cavitation number σ is verified to be small. Linear extrapolation then yields the drag coefficient at $\sigma=0$.

ANALYSIS AND CONCLUSIONS

In order to check the accuracy of the proposed model, several numerical test cases have been computed. In Figures 2 and 3 the numerical results for parabolic shapes with fineness ratio D/L between 0 and 1 are presented and Figures 4–8 give the results for conical shapes.

High-speed water tunnel experiments[9] show that the front part of the cavity interface is almost parabolic and the pressure inside the cavitation interface is approximately constant. Johnson and Rasnick[6] use the analytic expression of the potential flow field of a fully immersed ellipsoid to compute the drag force of a parabolic wetted nose in a cavitation flow regime. The authors show that in the limiting case when the eccentricity of the ellipsoid becomes large, the front part is almost parabolic and the pressure along it decays rapidly to the free stream pressure. Therefore the force acting on the frontal part of such an ellipsoid can be related to the drag force on a parabolic nose shape in cavitation flow at $\sigma=0$.[6] In Figure 2 the values computed using the

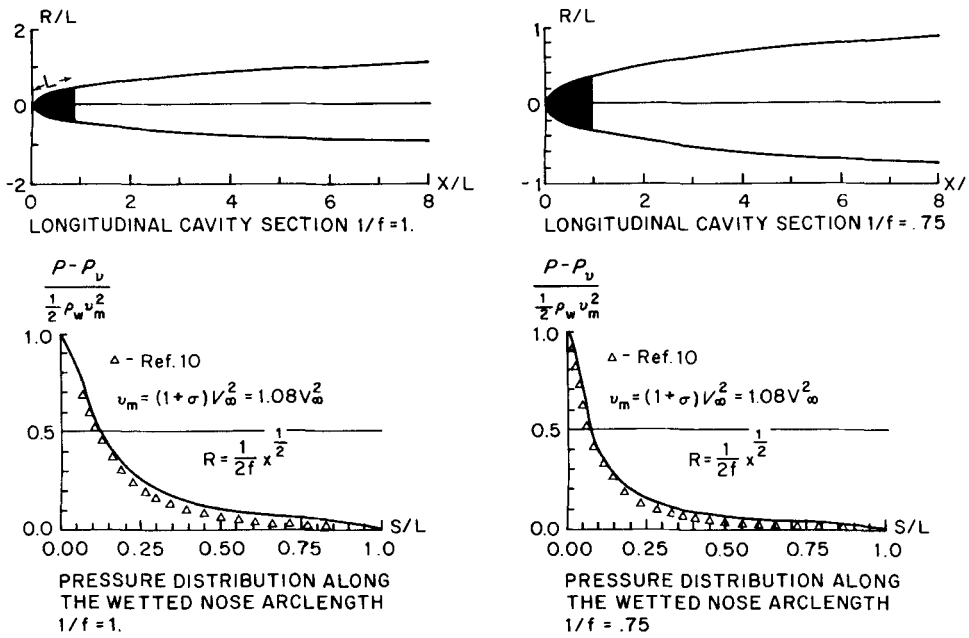

Figure 2. Longitudinal cavity section (top) and pressure distribution (bottom) for a wetted nose, with arc length $1/f=1$ (left) and $1/f=0{\cdot}75$ (right)

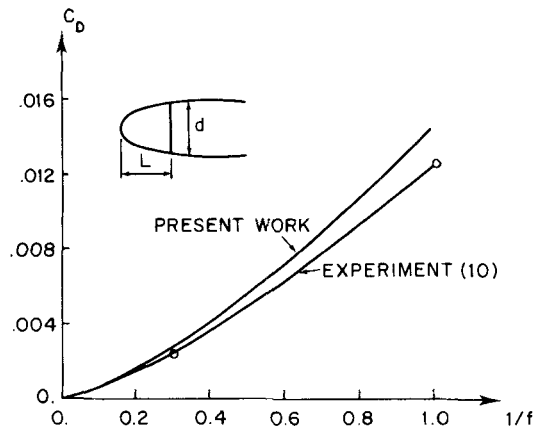

Figure 3. Drag of a parabolic nose; $\sigma=0$

present method at $\sigma=0{\cdot}08$ are compared with the results derived in Reference 6. In Figure 3 the computed drag coefficients for parabolic bodies are compared with the high-speed water experiments.[9] The computed pressure distribution along a disc interface is shown in Figure 5 and is compared with the numerical results obtained by Brennen.[2]

An experimental expression is proposed by May[9] for the cavity interface generated behind a

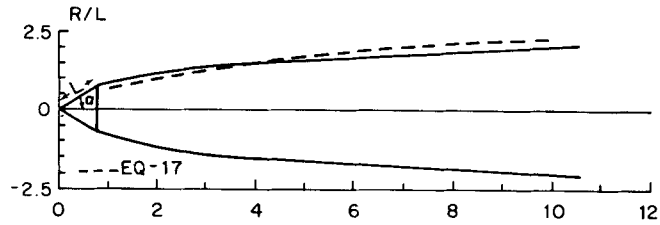

Figure 4. Cavity shape for a 45° cone

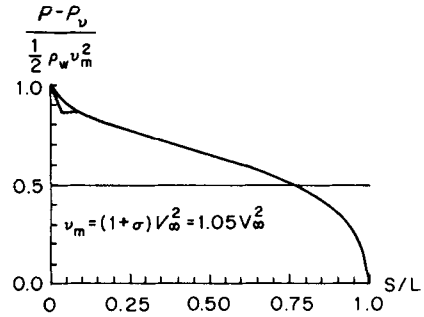

Figure 5. Pressure distribution for a 45° cone

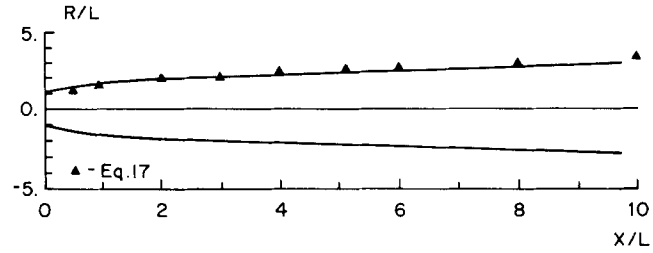

Figure 6. Cavity shape for a disc

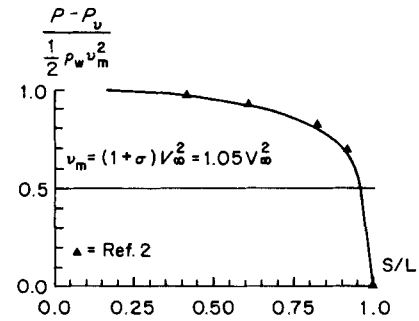

Figure 7. Pressure distribution for a disc

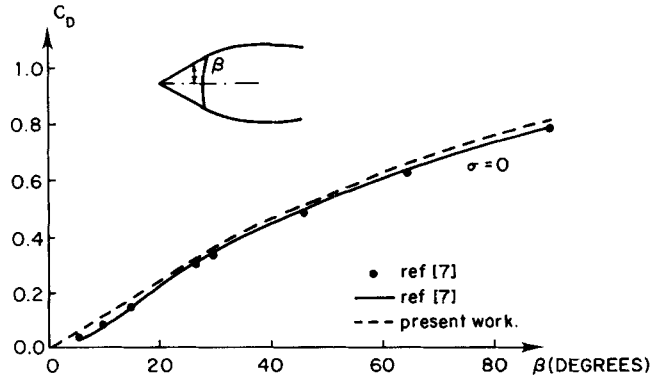

Figure 8. Comparison of numerical drag results with experimental results for a cone; $\sigma=0$

cone:

$$\left(\frac{R}{C_{d,0}^{1/2}d}\right)^2=0{\cdot}583\frac{x+a}{C_{d,0}^{1/2}d}, \tag{17}$$

where a/d and $C_{d,0}^{1/2}$ are given in Table II for a disc, a sphere and a cone.

The numerical results obtained in this research at $\sigma=0{\cdot}05$ are compared with expression (17) and good agreement is obtained for a cone and a disc, as illustrated in Figures 4 and 6 respectively.

The drag coefficient obtained in this research for a disc at $\sigma=0$ is 0·820 for 21 mesh points along the wetted nose, compared with 0·827,[1] 0·823 (Armstrong, from Reference 9) and 0·824 (Fisher, from Reference 9).

The sensitivity of the numerical algorithm is checked by increasing the number of mesh points along the wetted head forms: 21 mesh points are found to give stable results for a disc, while for parabolic head forms 38 mesh points are needed.

Good agreement is found between the drag coefficient obtained in this work and the experimental results[9] at $\sigma=0$. This comparison is illustrated in Figure 8, where the broken curve denotes the numerical results obtained in this research and the full curve denotes the best line through the experimental data.[9]

A smooth solution is obtained for a disc, while a local inaccuracy near the stagnation point appears in the solution for conical head forms at semi-cone angles less then 0·9 rad, resulting from inaccurate interpolation of the induced-velocity terms (f and g in equation (12)). The local inaccuracy has no effect on the overall solution (this has been checked by increasing the number of mesh points along the wetted nose), but it increases as a function of the wetted-nose slenderness. Such a local inaccuracy has not been observed for blunt wetted bodies (Figure 7).

In conclusion, the method of vortex ring distributions appears to work well and to produce good results. A considerable saving in computer time can be achieved by using a varying mesh interval in the integration scheme, as well as by a correct representation of the functions f and g in the vicinity of the stagnation point. Possibly, an alternative approach to remove this difficulty is by using a refined integration method, in a fashion similar to the method proposed in Reference 5. The present numerical algorithm can be extended to compute the axial cavitation flow at any cavitation number by using the Riabouchinski model. However, such an option has not been included in the present study and will probably appear in a future work.

Table II

'Wetted nose' form	a/d	$C_{d,0}^{1/2}$
Disc	0·4	0·898
Sphere	0·5	0·515
Cone (45° half-angle)	−0·2	0·707

It is worth noting that in the present work the computer memory required is only that for one square matrix of size equal to the number of mesh points along the wetted nose and a vector that contains the cavity interface ordinates. The methods of References 2 and 3 require larger matrices, for which the dimensions are given by the number of mesh points along B.

REFERENCES

1. P. R. Garabedian, 'Calculation of axially symmetric cavities and jets', *Stanford University Applied Math. Statist. Lab. Report 42*, 1955.
2. C. Brennen, 'A numerical solution of axisymmetric cavity flows', *J. Fluid Mech.*, **37**, part 4, 671–688 (1969).
3. T. R. Mogel and R. L. Street, 'A numerical method for steady cavity flows', *J. Ship Res.* **18**(1), 22–31 (1974).
4. A. H. Armstrong and J. H. Dunham, 'Axisymetric cavity flow', *Armament Research Establishment Report 12/53, London*, 1953.
5. M. I. Nove, M. Kurovmaru and S. Yamaguchi, 'A method of singularity with spline fit distribution for potential flow problems', *Memoirs of the faculty of Engineering, Kyushu University*, **37**(2), 89–106 (1977).
6. V. E. Johnson and T. A. Rasnick, 'The drag coefficient of parabolic bodies of revolution operating at zero cavitation number and zero angle of yaw', *NASA, Langley Research Center, Technical Report R-86*, 1961.
7. Van Te Chu, *Advances in Hydroscience, Vol. 1*, Academic Press, New York, 1964.
8. V. H. Arakeri, 'Viscous effects on the position of cavitation separation from smooth bodies', *J. Fluid Mech.*, **68**, part 4, 779–799 (1975).
9. A. May, 'Water entry and cavity running behaviour of missiles', *Navsea Hydrobalistics Advisory Commitee, Silver Spring, Maryland, Report Beavac/Tr75-2*, 1975.
10. H. Lamb, *Hydrodynamics*, Dover, New York, 1932.
11. M. Abramowitz and I. A. Stegun, *Handbook of Mathematical Functions*, Dover, New York, 1970.